Synthesis, bioevaluation and docking studies of new imidamide derivatives as nitric oxide synthase inhibitors

Fabio Arias [a], Francisco Franco-Montalban [a], Miguel Romero [b,c,d,e], M. Dora Carrión [a,*,1], M. Encarnación Camacho [a,*,1]

[a] Departamento de Química Farmacéutica y Orgánica, Facultad de Farmacia, Universidad de Granada, Spain
[b] Departamento de Farmacología, Facultad de Farmacia, Universidad de Granada, Spain
[c] Instituto de Investigación Biosanitaria de Granada, ibs.GRANADA, Granada, Spain
[d] Department of Pharmacology, School of Pharmacy and Center for Biomedical Research (CIBM), University of Granada, 18071 Granada, Spain
[e] Ciber de Enfermedades Cardiovasculares (CIBERCV), Spain

ARTICLE INFO

ABSTRACT

In search of new Nitric Oxide Synthase (NOS) inhibitor agents, two isosteric series of derivatives with an imidamide scaffold (one of them with a hydroxyl group and the other with a carbonyl one) were synthesized and evaluated on inducible (iNOS) and neuronal (nNOS) isoforms. These compounds have been designed by combining a kynurenamine framework with an amidine moiety in order to improve selectivity for the inducible isoform. In general, the *in vitro* inhibitory assays exhibited better inhibition values on the iNOS isoform, being the *N*-(3-(2-amino-5-methoxyphenyl)-3-hydroxypropyl)-4-(trifluoromethyl)benzimidamide **4i** the most active inhibitor with the highest iNOS selectivity, without inhibiting eNOS. Docking studies on the two most active compounds suggest a different binding mode on both isozymes, supporting the experimentally observed selectivity towards the inducible isoform. Physicochemical *in silico* studies suggest that these compounds possess good drug-likeness properties.

1. Introduction

Nitric oxide (NO) is a heterodiatomic molecule with an unpaired electron which behaves as a free radical. Its small size, lack of charge, and high solubility, allow NO to freely diffuse through any cellular membrane in the organism.[1]

NO is produced by the Nitric Oxide Synthase (NOS) during the transformation of L-arginine to L-Citrulline, consuming NADPH and O_2. There are three different isoforms named according to the place where they can be found: neurons (nNOS), endothelium (eNOS) or induced by the immune system (iNOS), being involved, respectively, in neurotransmission, smooth tissue relaxation and the immune response.[2]

Dysregulated NO levels are implicated in different disorders.[3] For example, the overproduction of NO by nNOS has been proven as a common factor in a wide range of neurological deficits such as Alzheimer's, Huntington's, Parkinson's, and amyotrophic lateral sclerosis.[4] Whereas, iNOS overexpression highly increases the NO levels, which later reacts with superoxide radical to produce reactive nitrogen species

(RNSs). These RNSs take part in several inflammatory and/or oxidative stress pathways, contributing in the development of various pathological conditions such as Parkinson's disease, Alzheimer's disease,[5,6] sepsis, heart failure,[7] multiple sclerosis,[8] rheumatoid arthritis,[9] diabetes mellitus,[10] inflammatory bowel disease[11] and acute lung injury.[12]

Nowadays, the involvement of NO in cancer is well known, specially, how the iNOS activity affects tumour progression.[13,14] Thus, the increase in iNOS expression has been found in different cancer types, such as breast,[15] colon,[16] pancreatic[17] and lung[18] cancers, as well as in head and neck squamous carcinoma[19] glioblastoma,[20,21] and melanoma.[22]

The main role of eNOS isoform is producing NO in order to relax vasculature, inhibit platelet and white cell adhesion, prevent smooth muscle cell replication, promote angiogenesis, and control the expression of vascular endothelium growth factor (VEGF).[23,24] In this sense, eNOS inhibition can lead to severe hypertension or other cardiovascular disorders.

Currently, the exploration of potent and selective NOS inhibitors could signify a step forward in future therapies for pathologies involving

---

* Corresponding authors.
    E-mail addresses: dcarrion@ugr.es (M.D. Carrión), ecamacho@ugr.es (M.E. Camacho).
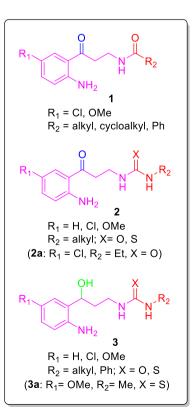   [1] These authors contributed equally.

NO overproduction. Thus, the development of selective nNOS inhibitors would be important to better understand the role of NO in the central nervous system and to deepen in the research of neurodegenerative disorders.[25] Besides, the investigation of selective iNOS inhibitors could be crucial for the research of new treatments for diseases where the immune and inflammatory response of the organism is involved, such as septic shock or rheumatoid artritis.[26]

Most compounds initially investigated as NOS inhibitors were designed mimicking the L-arginine structure, such as L-NAME (L-N^G-nitroarginine methyl ester). These molecules cannot be used clinically, since they are able to inhibit eNOS and, therefore, induce hypertension.[27] In order to find selective NOS inhibitors, we have already investigated different kynurenamine derivatives **1** (Fig. 1).[28] Afterward the substituted acyl group in compounds **1** was modified to obtain derivatives **2**[29] with a urea or thiourea moiety finding interesting molecules, such as the iNOS/nNOS selective oxopropyl-urea **2a** (R$_1$ = Cl, R$_2$ = Et, X = O; IC$_{50}$ = 100 μM in iNOS; IC$_{50}$ > 1000 μM in nNOS). Then, we have replaced the carbonyl group by a hydroxyl one, obtaining promising hydroxyproyl-ureas and thioureas **3**,[30] as derivative **3a** (R$_1$ = OMe, R$_2$ = Me, X = S; IC$_{50}$ = 180 μM in iNOS; IC$_{50}$ = 130 μM in nNOS). In the last years different aliphatic, aromatic and cyclic amidines have been studied as competitive iNOS inhibitors.[27] Thereby, in this paper we have investigated different derivatives with an amidine scaffold, and set a synthetic procedure to join two structural components, a kynurenamine skeleton with an imidamide residue. In vitro inhibition assays on iNOS and nNOS have been done on all synthesized compounds and the best performing molecules selected for the determination of its IC$_{50}$ values. Docking studies have also been carried out to account for the NOS isoform selectivity observed.

2. Results and discussion

2.1. Chemistry

Scheme 1 depicts the synthetic strategy adopted for the preparation of target compounds **4a-i** and **5a-h**. 5-Methoxy-2-nitrobenzaldehyde **6c** (synthesized by methylation with MeI and K$_2$CO$_3$),[31] along with the commercial 2-nitrobenzaldehyde **6a** and 5-chloro-2-nitrobenzaldehyde **6b**, were converted into the 3-(5-substituted-2-nitrophenyl)-3-hydroxypropanenitriles **7a-c** by treatment with *n*-BuLi and CH$_3$CN in dry THF. The nitrile group of these derivatives was reduced selectively with BH$_3$/THF to the primary amines **8a-c**.[30] For the next step, it was necessary to synthesize the benzyl-benzimidothioates **9b-d**, starting from benzyl bromide and the corresponding benzothioamides (Scheme 2).[32]

The reaction between the amine group of the distinct 3-amino-1-(2-nitro-5-substitutedphenyl)-propan-1-ols **8a-c** and the different imidates **9a-d**, which includes the commercially available ethyl acetimidate **9a**, generated the imidamide function present in the nine nitrophenylimidamide intermediates **10a-I**, which were turned into the final *N*-(3-(2-amino-5-substitutedphenyl)-3-hydroxypropyl)imidamides **4a-i** using Fe/FeSO$_4$ as reducing agent. In addition, the hydroxyl group of the diverse imidamides **10a-h** was oxidized to a carbonyl one with Jones reagent, to give the corresponding ketones **11a-h**. Finally, the nitro group of these intermediates were reduced to afford the final *N*-(3-(2-amino-5-substitutedphenyl)-3-oxopropyl)imidamides **5a-h**, as described for **4a-i**.

2.2. Biological activity evaluation

2.2.1. iNOS and nNOS inhibition

In order to elucidate the biological activity of the novel compounds as iNOS and nNOS inhibitors, *in vitro* assays employing human recombinant isoforms have been carried out. The data presented in Table 1 show the results of the preliminary inhibition screening for the final imidamides **4a-i** and **5a-h**. The tests were conducted at a terminal concentration of 1 mM in both isoforms. The range of values obtained oscillated between 16.22% and 99.61% in iNOS and between 7.18% and 89.16% in nNOS. Based on this preliminary evaluation, the new derivatives exhibited better inhibition values on the inducible isoform than on the neuronal one. In this sense, twelve molecules showed a
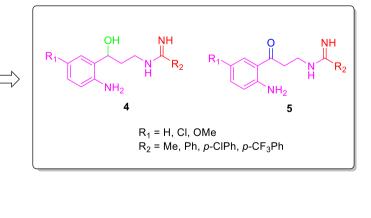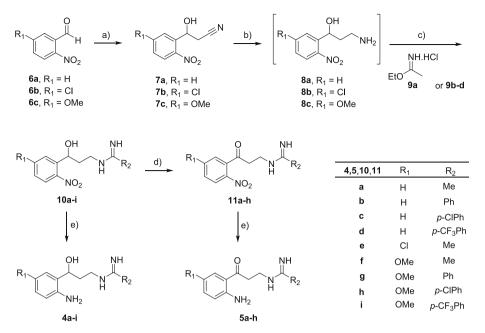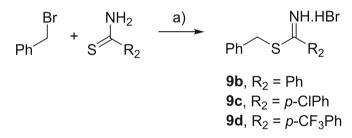

Fig. 1. Graphic overview of new imidamides described by our research group.

Scheme 1. Synthetic route of novel imidamides **4a-i** and **5a-h**. Reagents and conditions: a) CH_3CN, BuLi, THF, -78 °C, then RT; b) BH_3-THF, 0 °C, then 4 h RT; c) MeOH 0 °C, then 15 h RT; d) CrO_3, CH_3COCH_3, H_2SO_4, DCM 0 °C, 10 min; e) Fe/FeSO$_4$, H_2O, 100 °C, 1.5 h.

Scheme 2. Synthesis of benzimidothioates **9b-d**. Reagents and conditions: (a) $CHCl_3$, reflux 2 h.

Table 1
In vitro iNOS and nNOS inhibition (%) observed in the presence of 1 mM concentration of compounds **4a-i** and **5a-h**.

Compound	R_1	R_2	% iNOS inhibition[a]	% nNOS inhibition[a]
4a	H	Me	16.22 ± 1.89	28.26 ± 2.20
4b	H	Ph	64.09 ± 2.63	23.19 ± 1.88
4c	H	p-ClPh	73.17 ± 1.38	31.57 ± 0.82
4d	H	p-CF$_3$Ph	60.50 ± 2.33	36.45 ± 1.49
4e	Cl	Me	49.11 ± 1.25	66.11 ± 1.17
4f	OMe	Me	57.39 ± 1.42	19.01 ± 2.75
4g	OMe	Ph	95.91 ± 0.27	7.18 ± 2.81
4h	OMe	p-ClPh	81.02 ± 1.80	58.47 ± 0.69
4i	OMe	p-CF$_3$Ph	99.61 ± 0.55	12.50 ± 1.06
5a	H	Me	22.25 ± 0.84	88.83 ± 0.45
5b	H	Ph	35.63 ± 2.25	66.47 ± 1.02
5c	H	p-ClPh	33.42 ± 2.48	37.43 ± 1.67
5d	H	p-CF$_3$Ph	68.61 ± 1.28	55.98 ± 0.23
5e	Cl	Me	99.14 ± 0.69	19.88 ± 0.57
5f	OMe	Me	97.59 ± 1.24	89.16 ± 0.61
5g	OMe	Ph	94.73 ± 0.50	85.86 ± 1.62
5h	OMe	p-ClPh	75.12 ± 1.46	86.44 ± 0.99
2a[b]	Cl	Et	78.63 ± 1.34	9.86 ± 3.17
3a[b]	OMe	Me	76.55 ± 0.33	80.55 ± 2.29

[a] Values are the mean ± SEM of the percentage of iNOS and nNOS inhibition produced by 1 mM concentration of each compound. Each value is the mean of three experiments performed by triplicate using recombinant iNOS and nNOS enzymes. [b] **2a**[29] and **3a**[30] were used as reference.

percentage of inhibition greater than 50% on iNOS while eight compounds inhibited nNOS also with percentages of inhibition greater than 50%. In general, molecules with a hydroxypropyl group (derivatives with general structure **4**) exhibited higher percentages of iNOS inhibition, while those with a carbonyl rest (compounds type **5**) better inhibited the neuronal isoform.

Regarding the iNOS inhibition values, it can be seen that, in general, molecules with an electron-donating substituent in R_1 (OMe) show the highest inhibition rates versus this isozyme (**4g-i**, **5f-h**), except for **5e**, which has a high percentage of inhibition on iNOS and contains an electron-withdrawing group (R_1 = Cl).

With respect to neuronal isoform, derivatives **5f-h** (R_1 = OMe) behave as good nNOS inhibitors, along with **5a** (R_1 = H).

Despite presenting such a large range of percentages, iNOS selectivity prevails in most of these compounds, with the exception of the last members of this family **5f-h**, where a greater inhibition in nNOS is observed.

Among all candidates, the best performing in terms of percentage of inhibition were selected for the evaluation of their IC$_{50}$ values on the inducible isoform and on the neuronal one (see Table 2). The IC$_{50}$ values observed for iNOS range between 20.0 and 59.7 μM. The most active iNOS inhibitors of all tested compounds are the 3-hydroxypropyl derivatives with a methoxy group in R_1, **4i** ($R_2 = p$-CF$_3$Ph, IC$_{50}$ = 20.0 μM) and **4g** (R_2 = Ph, IC$_{50}$ = 22.5 μM), also presenting selectivity toward nNOS. In addition, the oxopropyl derivative **5e** (R_1 = Cl, R_2 = Me)

Table 2
IC$_{50}$ values (μM) for the inhibition of iNOS and nNOS activities by the most potent imidamide derivatives **4g**, **4i**, **5a** and **5e-g**.

Compound	iNOS[a]	nNOS[a]
4g	22.5	>1000
4i	20.0	>1000
5a	>1000	324.7
5e	25.6	>1000
5f	59.7	223.3
5g	45.2	193.7
2a[b]	100	>1000
3a[b]	180	130

[a] Data obtained by measuring the percentage of inhibition on at least six concentrations of each compound.
[b] **2a**[29] and **3a**[30] were used as reference.

exhibited an iNOS inhibition value almost comparable to its previous isosters (IC$_{50}$ = 25.6 μM), maintaining selectivity for this isoform.

In nNOS, the IC$_{50}$ values obtained are significantly higher than on iNOS, being the molecules with a carbonyl rest the best inhibitors, ranging from 193.7 μM in **5g** to 324.7 μM for **5a**, the latter being the compound presenting the best selectivity on nNOS. In this way, the replacement of the hydroxyl moiety for a carbonyl one decreases the iNOS potency and the selectivity versus nNOS.

These two series of imidamide derivatives have been designed by isosteric replacement from the oxopropyl-ureas and tioureas of general structure **2**[29] and the hydroxypropyl-ureas and thioureas **3**[30], being the most active molecules in each series the oxopropylurea **2a** (R$_1$ = Cl, R$_2$ = Et, X = O; IC$_{50}$ = 100 μM in iNOS and selectivity versus nNOS) and the hydroxypropyl-thiourea **3a** (R$_1$ = OMe, R$_2$ = Me, X = S; IC$_{50}$ = 180 μM versus iNOS and 130 μM in nNOS) (Table 2). In this regard, the amidine residue in imidamides **4** and **5** improve de iNOS inhibition values when compared to their previous isosters **3** and **2**, in addition to the iNOS/nNOS selectivity regarding the hydroxypropyl-thioureas.

2.2.2. eNOS inhibition activity

As indicated above, the undesirable side effects for NOS inhibitors derive from the alteration of the endothelial isoform. Hence, in order to prove that our most potent inhibitor, does not affect the cardiovascular system, a functional test with **4i** was carried out. In this way, acetylcholine-induced endothelium-dependent relaxation has been studied using endothelium intact rat aortic rings. This classic cholinergic agonist activates eNOS by a calcium-dependent mechanism.[33] The endothelium-dependent relaxation to acetylcholine was not affected by **4i** (Fig. 2), confirming the absence of eNOS inhibition of this compound, whereas the non-selective NOS inhibitor L-NAME almost abolished this response.

2.2.3. Cell viability (cytitixicity determination)

We investigated the cell viability activity of compounds **4g**, **4i**, **5e** and **5g** using HUVECs. The tested concentrations were within the range of IC$_{50}$ values for the inhibition of iNOS activity by the most potent imidamide derivatives. We observed that these compounds had little toxicity, but not significant as compared with the control conditions, since only at higher concentration tested (500 μM) the cell viability is
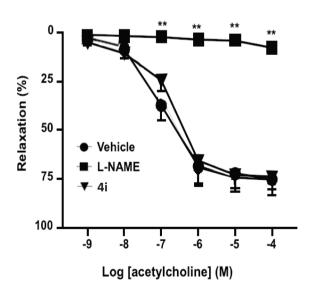
weakly (approximately 20%) reduced (Fig. 3).

2.3. Molecular docking study

Docking studies on human proteins iNOS and nNOS (pdb IDs 4CX7 and 6AV2) were performed to shed some light on the binding mode of these imidamide derivatives, and to account for the selectivity differences observed experimentally on both enzymes. Compounds were selected for the docking analysis as they perform best on the inhibition assays. Before any calculations were made, redocking of the cognate ligands on crystal structures 4CX7 and 6AV2 were carried out to account for the validity of docking protocol. In both cases, the preferred poses for the cognate ligands matched those of the crystal structures (results not shown). Next, compounds **4g** and **4i** were docked on human iNOS (pdb 4CX7) and nNOS (pdb 6AV2). Fig. 4a shows the preferred binding poses of both compounds on the catalytic active site of iNOS.

4g displays its phenyl ring underneath the Fe atom of the heme group favoring a π–cation interaction (Fig. 4a). Its imidamide group is displayed toward the carboxylate residues of the heme group forming a H-bond. Similarly, **4i** orients its *p*-CF$_3$Ph moiety directly underneath the Fe atom of the heme group, and because of its bulkier *p*-trifluorophenyl imidamide group, is forced to display the imidamide group away from the catalytic site and toward the carboxylate residues of the heme group. Unlike **4g**, **4i** can establish a H-bond with Gln263 at the entrance of the catalytic pocket. As these poses show, the imidamide groups of **4g** and **4i** are not binding the catalytic residue Glu377 as expected, however it should be noted the disposition of the *p*-methoxyaniline ring. In both compounds the ring is displayed toward a catalytic pocket generated by Gln263, Tyr347, Arg388, Asp382 and Tyr373, H-bonding the important catalytic residues Arg388, Asp382 and Tyr373.

These poses are of significance if we compare them with those adopted by NPA (N$^\omega$-propyl-L-arginine), and the natural substrate L-arginine, on the catalytic site of iNOS. Both compounds, **4g** and **4i**, show binding interactions with at least two of the catalytically important residues in the active site region.[34]

As for the binding poses of **4g** and **4i** on the nNOS they are shown in Fig. 4b. Like the poses seen on iNOS, in the neuronal model both compounds display their phenylimidamide moiety under the heme group, although with significant differences. **4i** and **4g** display its imidamide group toward Glu597 (Glu377 on iNOS) but no H-bonds are established with this residue. As for the *p*-methoxyaniline ring, and unlike the poses with the iNOS isozyme, both ligands display this moiety toward the carboxylic acids of the heme group, although only **4i** can H-bond the

Fig. 2. Effect of compound **4i** on eNOS activity. Acetylcholine-evoked relaxation in aortic rings with endothelium contracted with 1 μmol/L noradrenaline, after incubation with L-NAME (100 μM), **4i** (20 μM), or its vehicle (DMSO, 1/10^6) for 30 min. Data are expressed as mean ± SEM of n experiments. **P < 0.01 *vs.* rings incubated with vehicle.
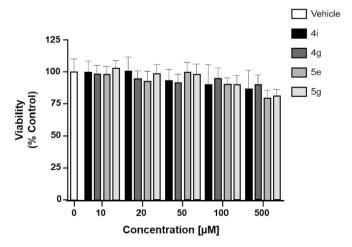

Fig. 3. Effect of compounds **4g**, **4i**, **5e** and **5g** on cell viability assessed by MTT reduction in HUVECs. Results were calculated as percentage of control (untreated cells) and data are presented as mean ± standard error of the mean (SEM) (n = 3 per group).
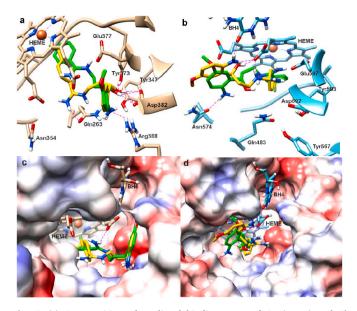
Fig. 4. (a) Superposition of predicted binding poses of **4g** (green) and **4i** (yelow) in iNOS (pdb ID 4CX7, tan). Hydrogen bonds are represented by dashed purple lines. (b) Superposition of predicted binding poses of **4g** (green) and **4i** (yelow) in nNOS (pdb ID 6AV2, blue). Hydrogen bonds are represented by dashed purple lines. (c). Superposition of the predicted binding poses of **4g** (green) and **4i** (yelow) in iNOS depicted as a Van der Waals surface. Red (negative charge), blue (positive charge), white (neutral). Heme group and BH_4 cofactor are represented as tan sticks and hydrogen bonds as dashed purple lines. (d) Superposition of the predicted binding poses of **4g** (green) and **4i** (yelow) in nNOS depicted as a Van der Waals surface. Red (negative charge), blue (positive charge), white (neutral). Heme group and BH_4 cofactor are represented as blue sticks and hydrogen bonds as dashed purple lines.

carboxylic moieties as well as the tetrahydrobiopterin (BH_4) cofactor. **4g** on the other hand, H-bond residue Asn574 (Asn354 on iNOS) at the entrance of the catalytic channel.

Although both poses are similar in terms of orientations, the reduced number of binding interactions in nNOS, and the tendency to bind the catalytically important pocket generated by residues Gln263, Tyr347, Arg388, Asp382 and Tyr373 in iNOS, might explain the low selectivity of both compounds toward nNOS found on the IC_{50} assays.

To account for the differences in orientation of **4g** and **4i** in both isozymes, the predicted binding poses are shown in Fig. 4c-d where the enzymes are represented as a Van der Waals surface. These pictures show the preference of the docked compounds to bid the region underneath the BH_4 cofactor and near the catalytic residues on iNOS, suggesting a higher selectivity toward this isozyme.

2.4. In silico prediction of physicochemical parameters and ADME properties

2.4.1. Physicochemical parameters

After potency and selectivity, another key aspect in the design of drugs is optimizing the administration route. A good strategy for predicting the oral bioavailability of a drug is to check if the compound meets the Lipinski and Veber rules. Lipinski's rules state that for a compound to be administered orally, it should meet at least three of the following conditions: (a) have a molecular weight below 500; (b) have an octanol–water partition coefficient below 5; (c) have no more than 5 hydrogen bond donor atoms; and (d) have no more than 10 hydrogen bond acceptor atoms.[35] Afterwards, Veber establishes additional rules for drug bioavailability: (a) the number of rotatable bonds must be less than 10, and (b) the polar surface area must be no greater than 140 Å^2.[36] In this article the Lipinski and Veber rules have been calculated for the compounds with the most interesting biological activity (**4g**, **4i**, **5e**, **5f**

and **5g**) using the free access website: https://www.molsoft.com/servers.html. These results are shown in Table 3. All compounds comply the Lipinski and Veber rules, so it could be predicted that they will present a high oral bioavailability.

2.4.2. ADME properties

The evaluation of the pharmacokinetic properties of absorption, distribution, metabolism and excretion are very important for developing a new therapeutic agent, to save time and costs. In order to calculate these properties in the most active compounds we have used the free access website: https://preadmet.bmdrc.kr/. These results are shown in Table 4.

Human intestinal absorption is one of the most important parameters in drug discovery. It is considered high absorption: 70–100%, medium absorption: 20–70% and low absorption: 0–20%.[37] These compounds have a high intestinal absorption which reinforces the theory that they could be good candidates for the design of oral drugs. Penetration through the blood–brain barrier can be advantageous if the drug exerts its effect on the central nervous system, but harmful if the drug acts only at the peripheral level. High penetration through the blood–brain barrier is considered >2, medium absorption 2-0.1, and low absorption <0.1.[37] The imidamide derivatives have shown moderate values of BBB penetration, in the case of the compounds **4g** and **4i** these values could be improved making a prodrug by the esterification of the hydroxyl group.

Plasma proteins binding could influence the half-life of a drug, since the protein-bound portion could act as a deposit of the drug that will be released slowly. A high union is estimated: >90%, and a weak union: <90.[37] According to theoretical calculations, the imidamide **4i** is the compound that shows the highest binding to plasma proteins.

CYP3A4 and CYP2C19 are cytochrome P450 enzymes responsible for drug metabolism, the inhibition of these proteins could cause an increase in plasma levels and toxicity. The *in silico* calculations indicate that these compounds are not inhibitors of these cytochromes.

A drug-like score is a value that indicates theoretically the similarity of a compound to a known therapeutic agent. A score of 1 shows that the compound is a good candidate to be a therapeutic agent.[38] Derivatives **4g** and **4i** present predicted values very close to 1, which is a good theoretical data in the development of new drugs.

3. Conclusions

Along this paper, the successful synthetic route for seventeen novel molecules has been described. In this process, two well-known structures in NOS inhibition: the imidamide core and kynurenamine skeleton have been fused, introducing at the same time, several moieties with different electronic characteristics. These modifications allowed us to study the way each one affected the activity. All final compounds were subjected to an inhibition screening on the neuronal and inducible NOS isoforms, selecting those with highest inhibition percentages for further

Table 3

Calculated Lipisnki and Veber parameters for compounds **4g**, **4i**, **5e**, **5f** and **5g**.

Comp.	MW	LogP	HBD	HBA	nVs	nRB	MolPSA
Lipinski*	≤500	≤5	≤5	≤10		–	–
Veber**	–	–	–	–	–	≤10	≤140
4g	299.16	1.65	5	3	0	7	72.40 Å^2
4i	367.15	2.71	5	3	0	8	72.40 Å^2
5e	239.08	1.49	4	2	0	5	72.40 Å^2
5f	235.13	0.84	4	3	0	6	70.08 Å^2
5g	297.15	2.16	4	3	0	7	69.49 Å^2

*Lipinski reference values; ** Veber reference values; MW, Molecular weight; LogP, lipophilicity (O/W); HBD, Number of hydrogen bond donors; HBA, Number of hydrogen bond acceptors; nVs, Number of Lipinski rule violations; nRB, Number of rotatable bonds; MolPSA, molecular polar surface area (PSA) (Å^2).

Table 4
ADME properties of compounds **4g**, **4i**, **5e**, **5f** and **5g**.

Comp.	HIA	BBB	PPB	CYP3A4 inhibition	CYP2C19 inhibition	Drug-likeness score
4g	78.52	0.29	51.65	Non	Non	0.93
4i	79.83	0.59	71.58	Non	Non	0.91
5e	79.77	0.74	3.38	Non	Non	−0.16
5f	68.28	0.20	10.40	Non	Non	−0.13
5g	81.52	0.36	55.23	Non	Non	0.28

HIA, Human Intestinal Absorption (%); BBB, Blood-Brain Barrier penetration; PPB, plasma protein binding; CYP3A4, Cytochrome P450 3A4; CYP2C19, Cytochrome P4502C19.

analysis in form of IC_{50}. The chosen ones were (**4h**, **4i**, **5e-g**) for iNOS, and (**5a**, **5f-g**) for nNOS, showing better inhibition values in the inducible isoenzyme, being **4g** (IC_{50} = 22.5 μM) and **4i** (IC_{50} = 20.0 μM) the best inhibitors. Using *in silico* models these compounds have shown an interesting oral bioavailability. Data obtained from docking studies on **4g** and **4i** reveal that these derivatives show their *p*-methoxyaniline ring toward an important catalytic pocket on iNOS establishing H-bond interactions with three vital residues, Gln263, Tyr373 and Asp382, meanwhile on nNOS the same scaffold shifts toward Asn574 (Asn354 on iNOS) at the entrance of the catalytic channel which could explain their iNOS selectivity. Furthermore, the cell viability test proved the absence of cytotoxicity in the most potent inhibitors at their IC_{50} values. Regarding the pharmacological experiments with aortic rat tissue, we can conclude that **4i** does not modify the relaxation associated to ACh making this compound an effective iNOS inhibitor. Moreover, this compound could be considered a new selective iNOS inhibitor for the development of new therapies for the treatment of inflammatory disorders, such as septic shock or rheumatoid arthritis, among others.

4. Experimental section

4.1. Chemistry

All starting materials, reagents and solvents, were commercially available. ^{1}H NMR and ^{13}C NMR spectra were obtained using Bruker Avance NEO spectrometers with Smart Probe BBFO equipped, operating at 400.57 MHz for ^{1}H and 100.73 MHz for ^{13}C, at 499.79 MHz for ^{1}H and 125.68 MHz for ^{13}C, or 600.25 MHz for ^{1}H and 150.95 MHz for ^{13}C, in the deuterated solvents. Chemical shifts are reported in ppm (δ ppm) and are referenced to the residual solvent peak. HRMS was conducted on a Waters LCT Premier Mass Spectrometer. Melting points were determined on an electrothermal melting point apparatus and were uncorrected.

General method for the synthesis of 3-(2-nitro-5-substitutedphenyl)3-hydroxypropanenitriles 7a-c. *n*-BuLi (1.6 M/hexane, 12.5 mL) was added to dry THF (20 mL) cooled to −78 °C under argon; then, acetonitrile (1.572 mL) was added dropwise. The mixture was stirred at −78 °C for 1 h. Afterward, a solution of the corresponding 2-nitrobenzaldehydes **6a-c** (10 mmol) in dry THF (10 mL) was added dropwise. The mixture was stirred again at −78 °C for 30 min and then warmed to RT. The mixture reaction was quenched with cold water (25 mL) and concentrated under vacuum. The crude was extracted with EtOAc (3 × 30 mL) and the organic phase was washed with NaHCO$_3$ saturated solution (15 mL) and brine (15 mL), dried over anhydrous Na$_2$SO$_4$, filtered and evaporated. The crude was purified by flash chromatography (EtOAc/hexane, 1: 4).

3-(2-Nitrophenyl)3-hydroxypropanenitrile (7a).[30] Yellow solid: mp: 82–85 °C; 93% yield.

3-(5-Chloro-2-nitrophenyl)3-hydroxypropanenitrile (7b).[30] Yellow solid; mp: 63–43 °C; 75% yield.

3-(5-Methoxy-2-nitrophenyl)3-hydroxypropanenitrile (7c).[30] Yellow solid: mp: 88–90 °C; 86% yield.

General method for the synthesis of 3-amino-1-(2-nitro-5-substitutedphenyl)-propan-1-ols 8a-c.[30] A solution of 1 M BH$_3$ (10 mL) in THF under argon was cooled to 0 °C and was added to the different 3-(2-nitro-5-substitutedphenyl)3-hydroxypropanenitriles **7a-c** (2.0 mmol) dropwise. The mixture was stirred for 5 h at RT. Afterward, the reaction mixture was cooled to 0 °C and an ice-cold solution of 6 N HCl (8.5 mL) was added carefully. The THF was evaporated, and the aqueous phase was basified with 10 M NaOH to pH = 8–9 and extracted with EtOAc (3 × 15 mL). The organic phase was washed with brine, dried over Na$_2$SO$_4$ and evaporated. The crude was used for the next step without purification.

General method for the synthesis of the benzyl-benzimidothioates 9b-d. Commercially available benzothioamides (benzothioamide, 4-chloro-benzothioamide or 4-(trifluoromethyl)benzothioamide) (5 mmol) were dissolved in CHCl$_3$ (15 mL); then, benzyl bromide (5.5 mmol, 634 μl) were added and the mixture was refluxed for 2 h. After cooling, the resulting white solid was filtered under vacuum.

Benzylbenzimidothioate hydrobromide (9b).[32] White solid; mp: 194–196 °C; 94% yield.

Benzyl 4-chlorobenzimidothioate hydrobromide (9c).[39] White solid; mp: 182–184 °C; 90% yield.

Benzyl 4-(trifluoromethyl)benzimidothioate hydrobromide (9d). White solid; mp: 147–145 °C; 79% yield. ^{1}H NMR (400 MHz, DMSO d_6): δ 11.02 (sa, 1H), 8.08 (d, J = 7.7 Hz, 2H), 8.00 (d, J = 7.7 Hz, 2H), 7.53 (d, J = 7.0 Hz, 2H), 7.39 (m, 3H), 4.75 (s, 2H). ^{13}C NMR (100 MHz, DMSO d_6) δ 166.68, 137.32, 135.01, 132.72, 129.39, 128.41, 128.34, 127.31, 125.26 (q, J = 3.4 Hz), 123.40 (q, J = 272.4 Hz), 41.58. HRMS (LSIMS): *m/z* calcd for C$_{15}$H$_{13}$NSF$_3$: 296.0721 [M + H]$^+$; found: 296.0733.

General method for the synthesis of N-(3-(2-nitro-5-substitutedphenyl)-3-hydroxypropyl)imidamides 10a-i. 3-Amino-1-(2-nitro-5-substitutedphenyl)propan-1-ol derivatives **8a-c** (2 mmol) were solved in MeOH (10 mL) and cooled to 0 °C; then, the different imidates **9a-d** (3 mmol) were added. The mixture was stirred for 15 h at room temperature. Afterward, the reaction mixture was evaporated and was purified by flash chromatography (DCM: MeOH, 9: 1 saturating with NH$_4$OH).

N-(3-Hydroxy-3-(2-nitrophenyl)propyl)acetimidamide (10a). Orange oil; 88% yield. ^{1}H NMR (400 MHz, CD$_3$OD) δ 7.90 (dd, J = 7.5 Hz, J = 4.7 Hz, 2H), 7.71 (t, J = 7.5 Hz, 1H), 7.48 (t, J = 7.5 Hz, 1H), 5.24 (d, J = 9.2 Hz, 1H), 3.60–3.42 (m, 2H), 2.26 (s, 3H), 2.19–2.07 (m, 1H), 1.95–1.84 (m, 1H). ^{13}C NMR (100 MHz, CD$_3$OD) δ 166.08, 148.74, 141.51, 134.70, 129.40, 129.11, 125.22, 67.34, 40.75, 37.29, 19.08. HRMS (LSIMS): *m/z* calcd for C$_{11}$H$_{15}$N$_3$O$_3$: 238.1192 [M + H]$^+$; found: 238.1178.

N-(3-Hydroxy-3-(2-nitrophenyl)propyl)benzimidamide (10b). Brown oil; 71% yield. ^{1}H NMR (400 MHz, DMSO d_6) δ 9.77 (sa, 1H), 9.48, 9.05 (sa, 1H), 7.91 (dd, J = 8.3 Hz, J = 1.1 Hz, 1H), 7.87 (dd, J = 7.9 Hz, J = 1.3 Hz, 1H), 7.81–7.67 (m, 4H), 7.61 (t, J = 7.6 Hz, 2H), 7.53 (dt, J = 8.3 Hz, J = 1.3 Hz, 1H), 5.78 (d, J = 4.5 Hz, 1H), 5.14 (m, 1H), 3.68–3.55 (m, 2H), 2.15–2.04 (m, 1H), 1.98–1.87 (m, 1H). ^{13}C NMR (100 MHz, DMSO d_6) δ 163.17, 147.36, 140.19, 133.49, 133.22, 129.14, 128.88, 128.34, 128.22, 128.15, 123.89, 65.40, 36.02, 30.70. HRMS (LSIMS): *m/z* calcd for C$_{16}$H$_{18}$N$_3$O$_3$: 300.1348 [M + H]$^+$; found: 300.1343.

4-Chloro-N-(3-hydroxy-3-(2-nitrophenyl)propyl)benzimidamide (10c). Orange oil; 70% yield. ^{1}H NMR (500 MHz, CD$_3$OD) δ 8.02 (ddd, J = 8.2 Hz, J = 2.9 Hz, J = 1.2 Hz, 2H), 7.87 (d, J = 8.7 Hz, 2H), 7.82 (dt, J = 7.4 Hz, J = 1.2H, 1H), 7.71 (d, J = 8.7 Hz, 2H), 7.58 (dt, J = 7.5 Hz, J = 1.5 Hz, 1H), 5.42 (dd, J = 9.6 Hz, J = 2.4 Hz, 1H), 3.90–3.84 (m, 1H), 3.80–3.75 (m, 1H), 2.38–2.31 (m, 1H), 2.12–2.05 (m, 1H). ^{13}C NMR (125 MHz, CD$_3$OD) δ 165.01, 148.81, 141.67, 140.74, 134.81, 130.83, 130.80, 130.58, 129.50, 129.19, 129.23, 125.30, 67.50, 41.50, 37.29. HRMS (LSIMS): *m/z* calcd for C$_{16}$H$_{17}$N$_3$O$_3$Cl: 334.0958 [M + H]$^+$; found: 334.0987.

N-(3-Hydroxy-3-(2-nitrophenyl)propyl)-4-(trifluoromethyl)benzimidamide (10d). Yellow oil; 96% yield. ^{1}H NMR (400 MHz, DMSO d_6) δ 9.98 (sa, 1H), 9.60, 9.35 (sa, 1H), 7.98 (dd, J = 26.1 z Hz, J = 8.3 Hz, 4H),

7.91 (d, J = 8.4 Hz, 1H), 7.86 (d, J = 7.5 Hz, 1H), 7.76 (t, J = 7.5 Hz, 1H), 7.52 (t, J = 7.5 Hz, 1H), 5.82 (sa, 1H), 5.13 (dd, J = 9.2 Hz, J = 2.1 Hz, 1H), 3.62 (m, 2H), 2.15–2.05 (m, 1H), 1.99–1.88 (m, 2H). ^{13}C NMR (100 MHz, DMSO d_6) δ 162.20, 147.36, 140.19, 133.52, 133.14 (d, J = 1.0 Hz), 132.72 (q, J = 32.5 Hz), 129.40, 128.37, 128.22, 125.77 (q, J = 3.7 Hz), 123.92, 123.56 (q, J = 272.8 Hz), 65.45, 40.02, 35.94. HRMS (LSIMS): m/z calcd for C$_{17}$H$_{17}$N$_3$O$_3$F$_3$: 368.1222 [M + H]$^+$; found: 368.1218.

N-(3-(5-Chloro-2-nitrophenyl)-3-hydroxypropyl)acetimidamide **(10e)**. Orange oil; 67% yield. ^{1}H NMR (500 MHz, CD$_3$OD) δ 8.00 (d, J = 8.7 Hz, 1H), 7.91 (d, J = 2.3 Hz, 1H), 7.51 (dd, 1H, J = 8.7 Hz, J = 2.3 Hz, 1H), 5.27 (dd, J = 9.5 Hz, J = 2.3 Hz, 1H), 3.60–3.45 (m, 2H), 2.41–2.29 (m, 1H), 2.26 (s, 3H), 1.91–1.78 (m, 1H). ^{13}C NMR (125 MHz, CD$_3$OD) δ 166.20, 146.99, 144.35, 141.08, 129.51, 129.18, 127.46, 67.24, 40.55, 37.15, 19.04. HRMS (LSIMS): m/z calcd for C$_{11}$H$_{15}$N$_3$O$_3$Cl: 272.0796 [M + H]$^+$; found: 272.0789.

N-(3-Hydroxy-3-(5-methoxy-2-nitrophenyl)propyl)acetimidamide **(10f)**. Brown oil; 68% yield. ^{1}H NMR (400 MHz, CD$_3$OD) δ 8.08 (d, J = 9.1 Hz, 1H), 7.44 (d, J = 2.7 Hz, 1H), 7.00 (dd, J = 9.1 Hz, J = 2.7 Hz, 1H), 5.42 (dd, J = 9.3 Hz, J = 2.0 Hz, 1H), 3.93 (s, 3H), 3.60–3.50 (m, 2H), 2.28 (s, 3H), 2.21–2.08 (m, 1H), 1.90–1.76 (m, 1H). ^{13}C NMR (100 MHz, CD$_3$OD) 166.14, 165.50, 145.66, 141.24, 128.65, 114.16, 113.65, 67.68, 56.59, 40.71, 37.29, 19.07. HRMS (LSIMS): m/z calcd for C$_{12}$H$_{18}$N$_3$O$_4$: 268.1297 [M + H]$^+$; found: 268.1292.

N-(3-Hydroxy-3-(5-methoxy-2-nitrophenyl)propyl)benzimidamide **(10g)**. Brown oil; 74% yield. ^{1}H NMR (500 MHz, CD$_3$OD) δ 8.14 (d, J = 9.1 Hz, 1H), 7.88 (d, J = 7.3 Hz, 3H), 7.78 (t, J = 7.5 Hz, 1H), 7.68 (t, J = 7.8 Hz, 2H), 7.53 (d, J = 2.8 Hz, 1H), 7.05 (dd, J = 9.1 Hz, J = 2.8 Hz, 1H), 5.59 (dd, J = 9.4 Hz, J = 2.1 Hz, 1H), 3.98 (s, 3H), 3.93–3.87 (m, 1H), 3.83–3.77 (m, 1H), 2.39—2.31 (m, 1H), 2.06–1.98 (m, 1H). ^{13}C NMR (125 MHz, CD$_3$OD) δ 165.84, 165.51, 145.67, 141.13, 134.61, 130.57, 130.36, 128.96, 128.70, 114.21, 113.70, 67.80, 56.66, 41.43, 37.24. HRMS (LSIMS): m/z calcd for C$_{17}$H$_{20}$N$_3$O$_4$: 330.1454 [M + H]$^+$; found: 330.1449.

4-Chloro-N-(3-hydroxy-3-(5-methoxy-2-nitrophenyl)propyl)benzimidamide **(10h)**. Orange oil; 76% yield. ^{1}H NMR (500 MHz, CD$_3$OD) 8.14 (d, J = 9.1 Hz, 1H), 7.85 (d, J = 8.7 Hz, 2H), 7.68 (d, J = 8.7 Hz, 2H), 7.51 (d, J = 2.8 Hz, 1H), 7.04 (dd, J = 9.1 Hz, J = 2.8 Hz, 1H), 5.55 (dd, J = 10.4 Hz, J = 2.1 Hz, 1H), 3.97 (s, 3H), 3.92–3.82 (m, 1H), 3.79–3.72 (m, 1H), 2.37–2.27 (m, 1H), 2.04–1.94 (m, 1H). ^{13}C NMR (125 MHz, CD$_3$OD) δ 165.58, 165.02, 145.74, 141.21, 140.76, 130.78, 130.57, 129.27, 128.73, 114.21, 113.71, 67.79, 56.62, 41.50, 37.22. MS (LSIMS): m/z calcd for C$_{17}$H$_{18}$N$_3$O$_4$Cl: 364.1059 [M + H]$^+$; found: 364.1051.

N-(3-Hydroxy-3-(5-methoxy-2-nitrophenyl)propyl)-4-(trifluoromethyl) benzimidamide **(10i)**. Orange oil; 68% yield. ^{1}H NMR (500 MHz, CD$_3$OD) δ 8.14 (d, J = 9.1 Hz, 1H), 8.02 (d, J = 8.3 Hz, 2H), 7.97 (d, J = 8.3 Hz, 2H), 7.51 (d, J = 2.8 Hz, 1H), 7.04 (dd, J = 9.1 Hz, J = 2.8 Hz, 1H), 5.54 (dd, J = 9.4 Hz, J = 2.1 Hz, 1H), 3.97 (s, 3H), 3.91–3.84 (m, 1H), 3.79–3.73 (m, 1H), 2.36–2.28 (m, 1H), 2.01–1.94 (m, 1H). ^{13}C NMR (125 MHz, CD$_3$OD) δ 165.66, 165.07, 145.80, 141.29, 135.75 (q, J = 33.0 Hz), 134.56 (d, J = 1.2 Hz), 130.09, 128.78, 127.28 (q, J = 3.8 Hz), 124.92 (q, J = 272.1 Hz), 114.20, 113.74, 67.80, 56.59, 41.60, 37.20. HRMS (LSIMS): m/z calcd for C$_{18}$H$_{19}$N$_3$O$_4$F$_3$: 392.1328 [M + H]$^+$; found: 398.1332.

General method for the synthesis of N-(3-(2-nitro-5-substitutedphenyl)-3-oxopropyl)imidamides **11a-h.** On a solution of the corresponding alcohols **10a-h** (1.5 mmol) in acetone (15 mL) and DCM (15 mL), cooled to 0 °C, freshly prepared Jones reagent (8 mL, 2.67 M) was added dropwise. After 20 min, MeOH (10 mL) was added. Then, the green precipitate was removed by filtration. The reaction mixture was evaporated and was purified by flash chromatography (DCM: MeOH, 10:1 saturating with NH$_4$OH).

N-(3-(2-Nitrophenyl)-3-oxopropyl)acetimidamide **(11a)**. Orange oil; 72% yield. ^{1}H NMR (400 MHz, CD$_3$OD): δ 8.16 (d, J = 8.2 Hz, 1H), 7.87 (dd, J = 7.8 Hz, J = 7.3 Hz, 1H), 7.76 (dd, J = 8.2 Hz, J = 7.8 Hz, 1H),

7.70 (d, J = 7.3 Hz, 1H), 3.74 (t, J = 5.9 Hz, 2H), 3.31–3.25 (m, 2H), 2.28 (s, 3H). ^{13}C NMR (100 MHz, CD$_3$OD) δ 201.04, 166.23, 147.16, 137.68, 135.62, 132.48, 128.84, 125.52, 41.14, 37.94, 19.05. HRMS (LSIMS): m/z calcd for: C$_{11}$H$_{14}$N$_3$O$_3$ 236.1035 [M + H]$^+$; found: 236.1043.

N-(3-(2-Nitrophenyl)-3-oxopropyl)benzimidamide **(11b)**. Yellow oil; 88% yield. ^{1}H NMR (400 MHz, CD$_3$OD) δ 8.22 (dd, J = 8.2 Hz, J = 0.8 Hz, 1H), 7.91 (dt, J = 7.6 Hz, J = 3.8 Hz, 1H), 7.85–7.79 (m, 3H), 7.79–7.73 (m, 2H), 7.71–7.63 (m, 2H), 4.03–3.95 (m, 2H), 3.50–3.32 (m, 2H). ^{13}C NMR (100 MHz, CD$_3$OD) δ 201.25, 166.11, 147.24, 137.76, 135.69, 134.63, 132.53, 130.70, 130.35, 129.02, 128.89, 125.60, 38.58, 37.57. HRMS (LSIMS): m/z calcd for C$_{16}$H$_{16}$N$_3$O$_3$: 298.1192 [M + H]$^+$; found: 298.1187.

4-Chloro-N-(3-(2-nitrophenyl)-3-oxopropyl)benzimidamide **(11c)**. White solid; mp: 177–179 °C; 67% yield. ^{1}H NMR (400 MHz, CD$_3$OD) δ 8.20 (dd, J = 8.2 Hz, J = 0.9 Hz, 1H), 7.90 (td, J = 7.6 Hz, J = 0.9 Hz, 1H), 7.82 (d, J = 8.6 Hz, 2H), 7.67 (d, J = 8.6 Hz, 2H), 7.42 (dd, J = 7.6 Hz, J = 1.5 Hz, 1H), 7.31–7.27 (m, 1H), 3.96 (t, J = 5.8 Hz, 2H), 3.44 (t, J = 5.8 Hz, 2H). ^{13}C NMR (100 MHz, CD$_3$OD) δ 201.17, 165.02, 147.17, 140.75, 137.69, 135.68, 132.50, 130.82, 130.53, 129.19, 128.91, 125.56, 41.17, 38.72. HRMS (LSIMS): m/z calcd for C$_{16}$H$_{15}$N$_3$O$_3$Cl: 332.0802 [M + H]$^+$; found: 332.0791.

N-(3-(2-nitrophenyl)-3-oxopropyl)-4-(trifluoromethyl)benzimidamide **(11d)**. Orange oil; 71% yield. ^{1}H NMR (500 MHz, CD$_3$OD): δ 8.21 (d, J = 8.2 Hz, 1H), 7.98 (q, J = 8.7 Hz, 4H), 7.90 (t, J = 7.5 Hz, 1H), 7.79 (t, J = 7.8 Hz, 1H), 7.71 (d, J = 7.5 Hz, 1H), 3.98 (m, 2H), 3.35 (m, 2H). ^{13}C NMR (125 MHz, CD$_3$OD) δ 201.20, 165.08, 147.19, 137.74, 135.74, 135.71(q, J = 32.9 Hz), 134.47, 132.54, 130.13, 128.89, 127.22 (q, J = 3.5 Hz), 125.61, 124.90 (q, J = 271.8 Hz), 43.92, 38.73. HRMS (LSIMS): m/z calcd for C$_{17}$H$_{15}$N$_3$O$_3$F$_3$: 366.1066 [M + H]$^+$; found: 366.1082.

N-(3-(5-Chloro-2-nitrophenyl)-3-oxopropyl)acetimidamide **(11e)**. Orange oil; mp: 153–155 °C; 65% yield. ^{1}H NMR (400 MHz, CD$_3$OD) δ 8.23 (d, J = 8.6 Hz, 1H), 7.79 (dd, J = 8.6 Hz, J = 2.2 Hz, 1H), 7.77 (d, J = 2.2 Hz, 1H), 3.76 (t, J = 5.8 Hz, 2H), 3.31 (t, J = 5.8 Hz, 2H), 2.31 (s, 3H). ^{13}C NMR (125 MHz, CD$_3$OD) δ 198.31, 164.88, 143.97, 140.62, 138.12, 130.85, 127.40, 126.04, 39.84, 36.36, 17.65. HRMS (LSIMS): m/z calcd for C$_{11}$H$_{13}$N$_3$O$_3$Cl: 270.0645 [M + H]$^+$; found: 270.0629.

N-(3-(5-methoxy-2-nitrophenyl)-3-oxopropyl)acetimidamide **(11f)**. Yellow oil; 83% yield. ^{1}H NMR (500 MHz, CD$_3$OD): δ 8.22 (d, J = 9.2 Hz, 1H), 7.20 (dd, J = 9.2 Hz, J = 2.7 Hz, 1H), 7.11 (d, J = 2.7 Hz, 1H), 3.98 (s, 3H), 3.75 (t, J = 6.0 Hz, 2H), 3.24 (t, J = 6.0 Hz, 2H), 2.29 (s, 3H). ^{13}C NMR (125 MHz, CD$_3$OD): δ 201.20, 166.27, 166.16, 141.22, 139.28, 128.32, 116.51, 113.57, 57.21, 41.44, 37.92, 19.06. HRMS (LSIMS): m/z calcd for C$_{12}$H$_{16}$N$_3$O$_4$: 266.1141 [M + H]$^+$; found: 266.1147.

N-(3-(5-methoxy-2-nitrophenyl)-3-oxopropyl)benzimidamide **(11g)**. Brown oil; 74% yield. ^{1}H NMR (400 MHz, CD$_3$OD) δ 8.23 (d, J = 9.1 Hz, 1H), 7.83 (d, J = 7.6 Hz, 2H), 7.76 (t, J = 7.3 Hz, 1H), 7.64 (t, J = 7.5 Hz, 2H), 7.21 (dd, J = 9.1 Hz, J = 2.0 Hz, 1H), 7.13 (d, J = 2.0 Hz, 1H), 3.98 (s, 3H), 3.43–3.29 (m, 4H). ^{13}C NMR (100 MHz, CD$_3$OD) δ 201.35, 168.49, 166.16, 140.82, 139.18, 135.22, 128.90, 128.85, 128.62, 128.29, 116.71, 113.52, 57.30, 45.93, 35.80. HRMS (LSIMS): m/z calcd for C$_{17}$H$_{18}$N$_3$O$_4$: 328.1297 [M + H]$^+$; found: 328.1293.

4-Chloro-N-(3-(5-methoxy-2-nitrophenyl)-3-oxopropyl)benzimidamide **(11h)**. Brown oil; 76% yield. ^{1}H NMR (400 MHz, CD$_3$OD): δ 8.26 (d, J = 9.2 Hz, 1H), 7.82 (d, J = 8.5 Hz, 2H), 7.67 (d, J = 8.5 Hz, 2H), 7.24 (dd, J = 9.2, J = 2.7 Hz, 1H), 7.16 (d, J = 2.7 Hz, 1H), 4.01 (s, 3H), 3.97 (t, J = 5.6 Hz, 2H), 3.38–3.32 (m, 2H). ^{13}C NMR (100 MHz, CD$_3$OD) δ 201.28, 166.19, 165.15, 141.19, 140.79, 139.30, 130.83, 130.75, 129.32, 128.36, 116.51, 113.64, 57.21, 47.94, 38.60. HRMS (LSIMS): m/z calcd for C$_{17}$H$_{17}$N$_3$O$_4$Cl: 362.0908 [M + H]$^+$; found: 362.0919.

General method for the synthesis of N-(3-(2-amino-5-substitutedphenyl)-3-hydroxypropyl)imidamides **4a-i** and *N-(3-(2-amino-5-substitutedphenyl)-3-oxopropyl)imidamides* **5a-h.** A mixture of the nitro derivatives **10a-i** or **11a-h** (1 mmol) was dissolved in water (10 mL), then Fe powder (10 mmol) and FeSO$_4$ (1 mmol) were added. The reaction was heated under reflux for 1.5 h. Next, the suspension was filtered through Celite. The

aqueous solution was evaporated under vacuum and purified by flash chromatography (DCM: MeOH, 8:1 saturating with NH₄OH).

*N-(3-(2-Aminophenyl)-3-hydroxypropyl)acetimidamide (**4a**)*. Orange oil; 68% yield. ^{1}H NMR (400 MHz, CD₃OD) δ 7.14 (dd, *J* = 7.9 Hz, *J* = 1.1 Hz, 1H), 7.03 (dt, *J* = 7.9 Hz, *J* = 1.1 Hz, 1H), 6.74 (d, *J* = 7.9 Hz, 1H), 6.69 (dt, *J* = 7.9 Hz, *J* = 0.8 Hz, 1H), 4.64–4.59 (m, 1H) 3.47–3.32 (m, 2H), 2.22 (s, 3H), 2.20–2.05 (m, 2H). ^{13}C NMR (100 MHz, CD₃OD) δ 166.02, 146.12, 129.25, 129.12, 128.01, 119.27, 118.07, 70.82, 40.94, 34.49, 18.99. HRMS (LSIMS): *m/z* calcd for C₁₁H₁₇N₃O: 208.1450 [M + H]⁺; found: 208.1435.

*N-(3-(2-Aminophenyl)-3-hydroxypropyl)benzimidamide (**4b**)*. Yellow oil; 71% yield. ^{1}H NMR (500 MHz, CD₃OD) δ 7.75–7.72 (m, 1H), 7.71 (d, *J* = 7.8 Hz, 2H), 7.60 (t, *J* = 7.8 Hz, 2H), 7.18 (d, *J* = 7.4 Hz, 1H), 7.05 (td, *J* = 8.0, *J* = 1.5 Hz, 1H), 6.76 (dd, *J* = 8.0, *J* = 1.0 Hz, 1H), 6.71 (td, *J* = 7.4, *J* = 1.0 Hz, 1H), 4.91 (dd, *J* = 8.4 Hz, *J* = 5.0 Hz, 1H), 3.74–3.60 (m, 2H), 2.35–2.17 (m, 2H). ^{13}C NMR (125 MHz, CD₃OD) δ 165.79, 146.19, 134.62, 130.38, 129.34, 129.14, 128.90, 128.61, 128.07, 119.36, 118.14, 71.44, 41.79, 34.36. MS (LSIMS): *m/z* calcd for C₁₆H₁₉N₃O: 270.1606 [M + H]⁺; found: 270.1597.

*N-(3-(2-Aminophenyl)-3-hydroxypropyl)-4-chlorobenzimidamide (**4c**)*. Yellow oil; 69% yield. ^{1}H NMR (500 MHz, CD₃OD) δ 7.70 (dt, *J* = 8.7 Hz, *J* = 2.1 Hz, 2H), 7.64 (dt, *J* = 8.7 Hz, *J* = 2.4 Hz, 2H), 7.18 (dd, *J* = 7.4 Hz, *J* = 1.4 Hz, 1H), 7.06 (td, *J* = 7.8 Hz, *J* = 1.4 Hz, 1H), 6.77 (dd, *J* = 7.8 Hz, *J* = 1.1 Hz, 1H), 6.72 (td, *J* = 7.4 Hz, *J* = 1.1 Hz, 1H), 4.93–4.89 (m, 1H), 3.61 (t, *J* = 7.0 Hz, 2H), 2.36–2.20 (m, 2H). ^{13}C NMR (125 MHz, CD₃OD) δ 164.89, 146.34, 140.82, 130.69, 130.56, 129.38, 129.24, 129.03, 128.09, 119.30, 118.11, 71.53, 41.84, 34.24. HRMS (LSIMS): *m/z* calcd for C₁₆H₁₉N₃OCl: 304.1217 [M + H]⁺; found: 304.1189.

*N-(3-(2-Aminophenyl)-3-hydroxypropyl)-4-(trifluoromethyl)benzimidamide (**4d**)*. Yellow oil; 65% yield. ^{1}H NMR (500 MHz, CD₃OD) δ 7.94–7.88 (m, 4H), 7.19 (dd, *J* = 7.5 Hz, *J* = 1.5 Hz, 1H), 7.04 (td, *J* = 7.9 Hz, *J* = 1.5 Hz, 1H), 6.76 (dd, *J* = 7.9 Hz, *J* = 1.1 Hz, 1H), 6.71 (td, *J* = 7.5 Hz, *J* = 1.1 Hz, 1H), 4.93 (dd, *J* = 8.4 Hz, *J* = 5.2 Hz, 1H), 3.64 (t, *J* = 6.9 Hz, 2H), 2.35–2.22 (m, 2H). ^{13}C NMR (125 MHz, CD₃OD) δ 164.70, 146.14, 135.66 (q, *J* = 33.4 Hz), 134.33 (d, *J* = 1.4 Hz), 130.07, 129.32, 129.13, 128.08, 127.19 (q, *J* = 3.8 Hz), 124.88 (q, *J* = 271.6 Hz), 119.36, 118.13, 71.32, 41.97, 34.29. HRMS (LSIMS): *m/z* calcd for C₁₇H₁₉N₃OF₃: 338.1480 [M + H]⁺; found: 338.1504.

*N-(3-(2-Amino-5-chlorophenyl)-3-hydroxypropyl)acetimidamide (**4e**)*. Orange oil; 67% yield. ^{1}H NMR (400 MHz, CD₃OD) δ 7.06 (d, *J* = 2.5 Hz, 1H), 6.89 (dd, *J* = 8.5 Hz, *J* = 2.5 Hz, 1H), 6.61 (d, *J* = 8.5 Hz, 1H), 4.73 (t, *J* = 7.0 Hz, 1H), 3.41–3.24 (m, 2H), 2.14 (s, 3H), 2.03–1.95 (m, 2H). ^{13}C NMR (100 MHz, CD₃OD) δ 166.04, 145.08, 130.81, 128.75, 127.46, 123.30, 118.90, 69.82, 40.82, 34.38, 19.03. HRMS (LSIMS): *m/z* calcd for C₁₁H₁₇N₃OCl: 242.1060 [M + H]⁺; found: 242.1055.

*N-(3-(2-Amino-5-methoxyphenyl)-3-hydroxypropyl)acetimidamide (**4f**)*. Red oil; 68% yield. ^{1}H NMR (400 MHz, CD₃OD) δ 6.81 (d, *J* = 2.8 Hz, 1H), 6.79 (d, *J* = 8.7 Hz, 1H), 6.70 (dd, *J* = 8.7 Hz, *J* = 2.8 Hz, 1H), 4.96 (d, *J* = 3.4 Hz, 1H), 3.71 (s, 3H), 3.41–3.33 (m, 2H), 2.19 (s, 3H), 2.12–2.04 (m, 2H). ^{13}C NMR (100 MHz, CD₃OD) δ 166.07, 155.42, 136.55, 132.46, 120.65, 114.80, 113.89, 70.57, 56.14, 40.83, 35.01, 18.95. HRMS (LSIMS): *m/z* calcd for C₁₂H₂₀N₃O₂: 238.1556 [M + H]⁺; found: 238.1555.

*N-(3-(2-Amino-5-methoxyphenyl)-3-hydroxypropyl)benzimidamide (**4g**)*. Brown oil; 70% yield. ^{1}H NMR (500 MHz, CD₃OD) δ 7.77–7.72 (m, 3H), 7.62 (t, *J* = 7.8 Hz, 2H), 6.88 (d, *J* = 2.8 Hz, 1H), 6.78 (d, *J* = 8.6 Hz, 1H), 6.71 (dd, *J* = 8.6 Hz, *J* = 2.8 Hz, 1H), 4.95 (dd, *J* = 8.0 Hz, *J* = 5.3 Hz, 1H), 3.74 (s, 3H), 3.65 (t, *J* = 7.0 Hz, 2H), 2.30–2.23 (m, 2H). ^{13}C NMR (125 MHz, CD₃OD) δ 165.71, 154.55, 138.64, 134.61, 131.41, 130.56, 130.36, 128.90, 119.78, 114.81, 113.73, 70.80, 56.13, 41.71, 34.71. HRMS (LSIMS): *m/z* calcd for C₁₇H₂₂N₃O₂: 300.1712 [M + H]⁺; found: 300.1730.

*N-(3-(2-Amino-5-methoxyphenyl)-3-hydroxypropyl)-4-chlorobenzimidamide (**4h**)*. Brown oil; 71% yield. ^{1}H NMR (500 MHz, CD₃OD) δ 7.74 (d, *J* = 8.6 Hz, 2H), 7.65 (d, *J* = 8.6 Hz, 2H), 6.88 (d, *J* = 2.8 Hz, 1H), 6.77 (d, *J* = 8.6 Hz, 1H), 6.71 (dd, *J* = 8.6 Hz, *J* = 2.8 Hz, 1H), 4.95 (dd, *J* = 7.8 Hz, *J* = 5.4 Hz, 1H), 3.75 (s, 3H), 3.65 (t, *J* = 6.9 Hz, 2H), 2.32–2.22 (m, 2H). ^{13}C NMR (125 MHz, CD₃OD) δ 164.75, 154.44, 140.74, 138.87, 131.27, 130.74, 130.53, 129.14, 119.67, 114.80, 113.73, 70.74, 56.13, 41.79, 34.64. HRMS (LSIMS): *m/z* calcd for C₁₇H₂₁N₃O₂Cl: 334.1322 [M + H]⁺; found: 334.1313.

*N-(3-(2-Amino-5-methoxyphenyl)-3-hydroxypropyl)-4-(trifluoromethyl)benzimidamide (**4i**)*. Brown oil; 75% yield. ^{1}H NMR (500 MHz, CD₃OD) δ 7.96–7.91 (m, 4H), 6.89 (d, *J* = 2.9 Hz, 1H), 6.78 (d, *J* = 8.6 Hz, 1H), 6.72 (dd, *J* = 8.6 Hz, *J* = 2.9 Hz, 1H), 4.95 (dd, *J* = 8.0 Hz, *J* = 5.3 Hz, 1H), 3.75 (s, 3H), 3.67 (t, *J* = 6.9 Hz, 2H), 2.32–2.24 (m, 2H). ^{13}C NMR (125 MHz, CD₃OD) δ 164.73, 154.58, 138.67, 135.70 (q, *J* = 33.0 Hz), 134.37, 131.40, 130.08, 127.21 (q, *J* = 3.7 Hz), 124.90 (q, *J* = 272.4 Hz), 119.79, 114.81, 113.80, 70.81, 56.13, 41.89, 34.61 (C-2′). HRMS (LSIMS): *m/z* calcd for C₁₈H₂₁N₃O₂F₃: 368.1586 [M + H]⁺; found: 368.1573.

*N-(3-(2-Aminophenyl)-3-oxopropyl)acetimidamide (**5a**)*. Orange solid; mp: 130–133 °C; 88% yield. ^{1}H NMR (500 MHz, CD₃OD): δ 7.79 (dd, *J* = 8.2 Hz, *J* = 1.5 Hz, 1H), 7.30 (ddd, *J* = 8.4 Hz, *J* = 6.9 Hz, *J* = 1.5 Hz, 1H), 6.80 (dd, *J* = 8.4 Hz, *J* = 1.2 Hz, 1H), 6.65 (ddd, *J* = 8.2 Hz, *J* = 6.9 Hz, *J* = 1.2 Hz, 1H), 3.67 (t, *J* = 6.1 Hz, 2H), 3.40 (t, *J* = 6.1 Hz, 2H), 2.24 (s, 3H). ^{13}C NMR (125 MHz, CD₃OD) δ 199.90, 166.03, 152.81, 135.75, 131.97, 118.42, 118.05, 116.27, 38.72, 37.40, 18.87. HRMS (LSIMS): *m/z* calcd for C₁₁H₁₄N₃O: 206.1293 [M + H]⁺; found: 206.1291.

*N-(3-(2-Aminophenyl)-3-oxopropyl)benzimidamide (**5b**)*. Yellow oil; 69% yield. ^{1}H NMR (400 MHz, CD₃OD): δ 7.72 (dd, *J* = 8.2 Hz, *J* = 1.3 Hz, 1H), 7.65–7.60 (m, 2H), 7.59–7.56 (m, 1H), 7.48 (dd, *J* = 10.8 Hz, *J* = 4.4 Hz, 2H), 7.18 (ddd, *J* = 8.4 Hz, *J* = 7.0 Hz, *J* = 1.3 Hz, 1H), 6.70 (dd, *J* = 8.4 Hz, *J* = 1.1 Hz, 1H), 6.54 (ddd, *J* = 8.2 Hz, *J* = 7.0 Hz, *J* = 1.1 Hz, 1H), 3.76–3.69 (m, 2H), 3.31–3.25 (m, 2H). ^{13}C NMR (100, CD₃OD) δ 200.56, 165.62, 152.67, 135.62, 133.99, 132.10, 131.87, 130.18, 128.71, 118.38, 117.59, 116.30, 43.45, 39.72. HRMS (LSIMS): *m/z* calcd for C₁₆H₁₈N₃O: 268.1450 [M + H]⁺; found: 268.1440.

*N-(3-(2-Aminophenyl)-3-oxopropyl)-4-chlorobenzimidamide (**5c**)*. Brown oil; 75% yield. ^{1}H NMR (600 MHz, CD₃OD) δ 7.73 (d, *J* = 5.8 Hz, 1H), 7.54 (d, *J* = 8.5 Hz, 2H), 7.35 (d, *J* = 8.5 Hz, 2H), 7.18 (t, *J* = 8.0 Hz, 1H), 6.69 (d, *J* = 8.0 Hz, 1H), 6.54 (t, *J* = 8.0 Hz, 1H), 3.47 (t, *J* = 7.5 Hz, 2H), 2.91 (t, *J* = 7.5 Hz, 2H). ^{13}C NMR (150 MHz, CD₃OD) δ 202.69, 165.03, 152.54, 137.20, 136.76, 134.25, 132.23, 129.60, 129.56, 127.31, 118.04, 115.56, 40.53, 34.90. HRMS (LSIMS): *m/z* calcd for C₁₆H₁₇N₃OCl: 302.1060 [M + H]⁺; found: 302.1036.

*N-(3-(2-Aminophenyl)-3-oxopropyl)-4-(trifluoromethyl)benzimidamide (**5d**)*. Orange oil; 78% yield. ^{1}H NMR (400 MHz, CD₃OD): δ 8.22 (d, *J* = 7.6 Hz, 1H), 7.99 (q, *J* = 8.8 Hz, 4H), 7.91 (t, *J* = 7.6 Hz, 1H), 7.80 (t, *J* = 7.6 Hz, 1H), 7.72 (d, *J* = 7.6 Hz, 1H), 4.03–3.94 (m, 2H), 3.36–3.33 (m, 2H). ^{13}C NMR (100 MHz, CD₃OD) δ 201.18, 165.16, 147.24, 137.81, 135.78 (q, *J* = 33.2 Hz), 135.76, 134.53, 132.57, 130.13, 128.84, 127.23 (q, *J* = 3.5 Hz), 125.66, 124.92 (q, *J* = 271.7 Hz), 38.68, 37.78. HRMS (LSIMS): *m/z* calcd for C₁₇H₁₇N₃OF₃: 336.1324 [M + H]⁺; found: 336.1308.

*N-(3-(2-Amino-5-chlorophenyl)-3-oxopropyl)acetimidamide (**5e**)*. Orange oil; 78% yield. ^{1}H NMR (500 MHz, CD3OD): δ 7.73 (d, *J* = 2.4 Hz, 1H), 7.21 (dd, *J* = 8.9 Hz, *J* = 2.4 Hz, 1H), 6.79 (d, *J* = 8.9 Hz, 1H), 3.64 (t, *J* = 6.1 Hz, 2H), 3.35 (t, *J* = 6.1 Hz, 2H), 2.22 (s, 3H). ^{13}C NMR (125 MHz, CD3OD) δ 199.04, 166.01, 151.38, 135.53, 130.86, 120.16, 120.09, 118.36, 38.59, 37.46, 18.95. HRMS (LSIMS): *m/z* calcd for C₁₁H₁₅N₃OCl: 240.0904 [M + H]⁺; found: 240.0886.

*N-(3-(2-Amino-5-methoxyphenyl)-3-oxopropyl)acetimidamide (**5f**)*. Brown oil; 69% yield. ^{1}H NMR (400 MHz, CD3OD) δ 7.23 (d, *J* = 2.8 Hz, 1H), 7.01 (dd, *J* = 9.0 Hz, *J* = 2.8 Hz, 1H), 6.78 (d, *J* = 9.0 Hz, 1H), 3.78 (s, 3H), 3.66 (t, *J* = 6.1 Hz, 2H), 3.39 (t, *J* = 6.1 Hz, 2H), 2.23 (s, 3H). ^{13}C NMR (125 MHz, CD3OD) δ 199.50, 166.01, 151.24, 147.48, 125.13, 120.01, 117.82, 113.87, 56.45, 38.73, 37.58, 18.90. HRMS (LSIMS): *m/z* calcd for C₁₂H₁₈N₃O₂: 236.1399 [M + H]⁺; found: 236.1388.

*N-(3-(2-Amino-5-methoxyphenyl)-3-oxopropyl)benzimidamide (**5g**)*.

Orange oil; 84% yield. ^{1}H NMR (400 MHz, CD3OD): δ 7.80–7.74 (m, 3H), 7.64 (dd, J = 10.9 Hz, J = 4.5 Hz, 2H), 7.30 (d, J = 2.9 Hz, 1H), 7.05 (dd, J = 9.0 Hz, J = 2.9 Hz, 1H), 6.81 (d, J = 9.0 Hz, 1H), 3.91 (t, J = 6.2 Hz, 2H), 3.82 (s, 3H), 3.55 (t, J = 6.2 Hz, 2H). ^{13}C NMR (125 MHz, CD3OD) δ 199.81, 165.88, 151.27, 147.48, 134.60, 130.62, 130.34, 128.94, 125.20, 120.05, 117.91, 113.94, 56.51, 39.74, 37.66. HRMS (LSIMS): m/z calcd for $C_{17}H_{20}N_3O_2$: 298.1556 [M + H]$^+$; found: 298.1553.

N-(3-(2-Amino-5-methoxyphenyl)-3-oxopropyl)-4-chlorobenzimidamide (5h). Yellow oil; 83% yield. ^{1}H NMR (400 MHz, CD3OD): δ 7.76 (d, J = 8.5 Hz, 2H), 7.66 (d, J = 8.5 Hz, 2H), 7.29 (d, J = 2.7 Hz, 1H), 7.08 (dd, J = 9.0 Hz, J = 2.7 Hz, 1H), 6.85 (d, J = 9.0 Hz, 1H), 3.89 (t, J = 6.0 Hz, 2H), 3.81 (s, 3H), 3.35 (t, J = 6.0 Hz, 2H). ^{13}C NMR (100 MHz, CD3OD) δ 199.73, 164.97, 151.28, 147.51, 140.77, 130.76, 130.65, 130.55, 125.22, 120.04, 117.89, 113.96, 56.50, 47.94, 39.70. HRMS (LSIMS): m/z calcd for $C_{17}H_{19}N_3O_2Cl$: 332.1166 [M + H]$^+$; found: 332.1179.

4.2. In vitro nNOS and iNOS activity determination

Enzymatic inhibition determination of the final products was carried out following different procedures depending on each isoform of NOS. Most of the used compounds were supplied by Sigma-Aldrich (Merk), except the tritium-labeled L-[^{3}H]-arginine, from Amersham Biosciences (Perkin Elmer) and the human enzymes iNOS and nNOS recombinants, from Enzo Life Sciences (Taper).

In these two isoforms, the *in vitro* enzymatic activity tests were performed in triplicate, following the Bredt & Snyder methodology.[40]

The basic foundation of this methodology is the control of the conversion of L-[^{3}H]-arginine to L-[^{3}H]-citrulline, due to the use of a Beckman LS 6500 multi-purpose scintillation counter detector.

The final volume for each one of the replicates is 100 μl, of which: 50 μl correspond to a buffer solution containing 25 mM tris-(hydroxymethyl)-aminomethane hydrochloride (Tris-HCl), 1 mM DL-dithiothreitol (DTT), 4 μM 5,6,7,8-tetrahydro-L-biopterin dihydrochloride (BH₄), 10 μM flavin-adenine dinucleotide (FAD), 0.5 mM hypoxanthine-9-ribofuranoside (inosine), 0.5 mg/ml bovine serum albumin (BSA), 0.1 mM CaCl₂, 10 μM L-arginine, 10 μg/ml calmodulin (CaM) (only in nNOS) and 0.05 μM L-[^{3}H]-arginine, always maintaining a pH of 7.6; 10 μl of an aliquot of the NOS isoform correspondent to the study performed; 10 μl of a solution of the product to be evaluated; 10 μl of 7.5 mM NADPH (except in control wells); and, finally, enough H₂O MiliQ to reach 100 μl.

All samples are incubated for 30 min at 37 °C. After that, 400 μl of a low-temperature buffer is added to stop the enzymatic process. This solution contains 0.1 M *N*-(2-hydroxymethyl)piperazine-*N'*-(2-ethanesulfonic) (HEPES) acid, 10 mM ethylene glycol-bis-(2-aminoethyl ether)-*N,N,N',N'*-tetraacetic acid (EGTA) and 0.175 mg/ml L-citrulline at pH = 5.5.

The sudden drop in temperature, the pH change and the dilution of all the components found in the reaction well, are the main factors that cause the stop of the enzymatic reaction; in addition, EGTA is also capable of chelating the Ca^{2+} ions, essential for the dimerization and functioning of the enzyme.

After this stage, each sample is passed through a column with Dowex-50 W ion exchange resin (Na$^+$) and then washed with H₂O MiliQ (1.2 mL), thus losing about 98% of the radioactivity.

Finally, 50 μl of each replica are diluted in Eco Lite (+) scintillation liquid to take measurements the next day, once other factors capable of exciting the scintillation liquid beyond the β emissions are eliminated.

NOS activity is expressed in picomoles of L-citrulline produced per mg of protein per minute (pM/mg min).

For the statistical treatment of data, the Prism8 program of GraphPad was used, where the IC$_{50}$ calculation was carried out by means of non-linear regression ELISA studies with variable slope of four factors.

4.3. In vitro eNOS activity determination

In order to evaluate the eNOS activity, it has been necessary working with tissue from experimental animals. Regulations for the protection of animals used for scientific purposes of the European Union were followed to carry out this study. All experimental protocols were approved by the Animal Care and Ethics Committee of the University of Granada (Spain; permit no: 12/11/2017/164). Male Wistar rats (250–300 g), obtained from Harlam Laboratories SA (Barcelona, Spain), were euthanized by a quick blow on the head followed by exsanguination.

The descending thoracic aortic rings were dissected. Then, they were mounted in organ chambers filled with Krebs solution (composition in mM: NaCl, 118; KCl, 4.75; NaHCO₃, 25; MgSO₄, 1.2; CaCl₂, 2; KH₂PO₄, 1.2; and glucose, 11) at 37 °C and gassed with 95% O₂ and 5% CO₂ and were stretched to 2 g of resting tension by means of two L-shaped stainless-steel wires inserted into the lumen and attached to the chamber and to an isometric force–displacement transducer (UF-1, Cibertec, Madrid, Spain), and recorded in a recording and analysis system (MacLab ADInstruments), as described previously.[39]

Rings were then mounted in organ chambers filled with Krebs solution and were stretched to 2 g of resting tension by means of two L-shaped stainless-steel wires inserted into the lumen and attached to the chamber and to an isometric force–displacement transducer (UF-1, Cibertec, Madrid, Spain), and recorded in a recording and analysis system (MacLab ADInstruments), as described previously.[41]

After stabilization of the medium conditions, these rings were incubated with a known eNOS inhibitor: L-NAME (100 μM), the compound **4i** (20 μM), or its vehicle (DMSO, 1/10^6) for 30 min. The contraction was then induced by a [1 μM] norepinephrine solution. Once a plateau contraction was reached, a concentration–response curve was constructed by cumulative addition of acetylcholine. Results are expressed as percentage of norepinephrine-evoked contraction. Data are expressed as means ± standard error mean and n reflects the number of aortic rings from different rats. Statistically significant differences among groups were calculated by two-way ANOVA followed by a Dunnett's multiple comparison test. P < 0.05 was considered statistically significant.

4.4. Cell viability assay

To examine the cytotoxicity induced by compounds **4g**, **4i**, **5e** and **5f**, changes in the viability of HUVECs, after incubation with these compounds, were evaluated by assessing mitochondrial activity by the MTT reduction assay. Briefly, HUVECs were seeded at 1x10^4 cells per well in a 96-well microtiter plate and incubated at 37 °C for up to 24 h. Then, the cells supernatants were removed and replaced by fresh medium serum free for at least two hours before the cells were exposed to serial dilutions of compounds (10 - 500 μM) for 30 min. At the selected time, 20 uL of 5 mg/ml MTT in PBS was added to the cells and further incubated at 37 °C for 3 h. After washing, 100 μl of DMSO were added into each well, and the spectrophotometric analysis was run at 570 nm using a multi-well plate reader (Fluorostart; BMG Labtechnologies, Offenburg, Germany) with background subtraction at 630 nm. Cell viability was calculated as the percentage of the viable cells compared with untreated controls. The viability experiments were conducted in at least three independent times, each run in triplicate. Results are expressed as percentage relatively to the untreated condition.

4.5. Docking studies

4.5.1. Docking protocol

Docking studies were carried out with Autodock 4.2.6 (AD4)[42] on the iNOS and nNOS pdb IDs 4CX7 and 6AV2, respectively. Ligands structures were built on Avogadro[43] and optimized using Gaussian[44] (HF/6-31G(d,p)). Compounds presenting tertiary amines, prone to protonation at physiological pH, were also considered. Once optimized, ligands PDBs were prepared for docking using the prepare_ligand4.py script included

MGLTools 1.5.4.[42] Protein structures, on the other hand, were prepared for docking using the PDB2PQR tools.[45] Water and ligand molecules were removed and charges and non-polar hydrogen atoms were added at pH 7.0. The produced structures were saved as a pdb files and prepared for docking using the prepare_receptor4.py script from MGLTools. The Fe atom of heme was assigned a charge of $+3$. AD4 was used to automatically dock the ligands into the iNOS and nNOS binding sites. For both enzymes, the docking grid was centered on the ligand binding site and set with the following grid parameters: 60 Å × 60 Å × 60 Å with 0.375 Å spacing. In all calculations, AD4 parameter file was set to 100 GA runs, 2.500.000 energy evaluations and a population size of 150. The Lamarckian genetic algorithm local search (GALS) method was used for the docking calculations. All dockings were performed with a population size of 250 and a Solis and Wets local search of 300 rounds was applied with a probability of 0.06. A mutation rate of 0.02 and a crossover rate of 0.8 were used. The docking results from each of the 100 calculations were clustered based on root-mean square deviation (RMSD) solutions differing by less than 2.0 Å between the Cartesian coordinates of the atoms and ranked on the basis of free energy of binding.

Declaration of Competing Interest

Authors declare no interest conflict.

References

1 Vallance P, Leiper J. Blocking NO synthesis: how, where and why? *Nat Rev Drug Discov*. 2002;1:939–950. https://doi.org/10.1038/nrd960.

2 Mohamed MFA, Marzouk AA, Nafady A, et al. Design, synthesis and molecular modeling of novel aryl carboximidamides and 3-aryl-1,2,4-oxadiazoles derived from indomethacin as potent anti-inflammatory iNOS/PGE2 inhibitors. *Bioorg Chem*. 2020;105, 104439. https://doi.org/10.1016/j.bioorg.2020.104439.

3 Grottelli S, Amoroso R, Macchioni L, et al. Acetamidine-Based iNOS Inhibitors as Molecular Tools to Counteract Inflammation in BV2 Microglial Cells. *Molecules*. 2020;25:1–18. https://doi.org/10.3390/molecules25112646.

4 Cinelli MA, Reidl CT, Li H, Chreifi G, Poulos TL, Silverman RB. First Contact: 7-Phenyl-2-Aminoquinolines, Potent and Selective Neuronal Nitric Oxide Synthase Inhibitors That Target an Isoform-Specific Aspartate. *J Med Chem*. 2020;63:4528–4554. https://doi.org/10.1021/acs.jmedchem.9b01573.

5 Akiyama H, Barger S, Barnum S, et al. Inflammation and Alzheimer's disease. *Neurobiol Aging*. 2000;21:383–421. https://doi.org/10.1016/S0197-4580(00)00124-X.

6 Trippier PC, Labby KJ, Hawker DD, Mataka JJ, Silverman RB. Target- and mechanism-based therapeutics for neurodegenerative diseases: strength in numbers. *J Med Chem*. 2013;56:3121–3147. https://doi.org/10.1021/jm301592.

7 Minhas R, Bansal Y, Bansal G. Inducible nitric oxide synthase inhibitors: A comprehensive update. *Med Res Rev*. 2020;40:823–855. https://doi.org/10.1002/med.21636.

8 Smith KJ, Lassmann H. The role of nitric oxide in multiple sclerosis. *Lancet Neurol*. 2002;1:232–241. https://doi.org/10.1016/S1474-4422(02)00102-3.

9 Mateen S, Moin S, Zafar A, Khan AQ. Redox signaling in rheumatoid arthritis and the preventive role of polyphenols. *Clin Chim Acta*. 2016;463:4–10. https://doi.org/10.1016/j.cca.2016.10.007.

10 Francés DE, Ingaramo PI, Ronco MT, Carnovale CE. Diabetes, an inflammatory process: oxidative stress and TNFalpha involved in hepatic complication. *J Biomed Sci Eng*. 2013;(6):645–653. https://doi.org/10.4236/jbise.2013.66079.

11 Dijkstra G, Zandvoort AJH, Muller Kobold AC, et al. Increased expression of inducible nitric oxide synthase in circulating monocytes from patients with active inflammatory bowel disease. *Scand J Gastroenterol*. 2002;37:546–554. https://doi.org/10.1080/00365520252903099.

12 Tang L, Gao X, Zhao B, et al. Design and synthesis of new disubstituted benzoxazolone derivatives that act as iNOS inhibitors with potent anti-inflammatory activity against LPS-induced acute lung injury (ALI). *Bioorg Med Chem*. 2020;28, 115733. https://doi.org/10.1016/j.bmc.2020.115733.

13 Wang H, Wang L, Xie Z, et al. Nitric Oxide (NO) and NO Synthases (NOS)-Based Targeted Therapy for Colon Cancer. *Cancers*. 2020;12:1–25. https://doi.org/10.3390/cancers12071881.

14 Belgorosky D, Girouard J, Langle YV, et al. Relevance of iNOS expression in tumor growth and maintenance of cancer stem cells in a bladder cancer model. *J Mol Med*. 2020;98:1615–1627. https://doi.org/10.1007/s00109-020-01973-0.

15 Vahora H, Munawwar AK, Alalami U, Hussain A. The potential role of nitric oxide in halting cancer progression through chemoprevention. *J Cancer Prev*. 2016;21:1–12. https://doi.org/10.15430/JCP.2016.21.1.1.

16 Puglisi MA, Cenciarelli C, Tesori V, et al. High nitric oxide production, secondary to inducible nitric oxide synthase expression, is essential for regulation of the tumourinitiating properties of colon cancer stem cells. *J Pathol*. 2015;236:479–490. https://doi.org/10.1002/path.4545.

17 Singh S, Gupta AK. Nitric oxide: role in tumour biology and iNOS/NO-based anticancer therapies. *Cancer Chemother Pharmacol*. 2011;67:1211–1224. https://doi.org/10.1007/s00280-011-1654-4.

18 Prueitt RL, Boersma BJ, Howe TM, et al. Inflammation and IGF-I activate the Akt pathway in breast cancer. *Int J Cancer*. 2007;120:796–805. https://doi.org/10.1002/ijc.22336.

19 Pervin S, Singh R, Hernandez E, Wu G, Chaudhuri G. Nitric oxide in physiologic concentrations targets the translational machinery to increase the proliferation of human breast cancer cells: Involvement of mammalian target of rapamycin/eIF4E pathway. *Cancer Res*. 2007;67:289–299. https://doi.org/10.1158/0008-5472.CAN-05-4623.

20 Thomas DD, Ridnour LA, Espey MG, et al. Superoxide fluxes limit nitric oxide-induced signaling. *J Biol Chem*. 2006;281:25984–25993. https://doi.org/10.1074/jbc.M602242200.

21 Maccallini C, Arias F, Gallorini M, et al. Antiglioma Activity of Aryl and Amido-Aryl Acetamidine Derivatives Targeting iNOS: Synthesis and Biological Evaluation. *ACS Med Chem Lett*. 2020;11:1470–1475. https://doi.org/10.1021/acsmedchemlett.5b00149.

22 Thomas DD, Espey MG, Ridnour LA, et al. Hypoxic inducible factor 1α, extracellular signal-regulated kinase, and p53 are regulated by distinct threshold concentrations of nitric oxide. *Proc Natl Acad Sci USA*. 2004;101:8894–8899. https://doi.org/10.1073/pnas.0400453101.

23 Garcia V, Sessa WC. Endothelial NOS: perspective and recent developments. *Br J Pharmacol*. 2019;176:189–196. https://doi.org/10.1111/bph.14522.

24 Maccallini C, Mollica A, Amoroso R. The positive regulation of eNOS signaling by PPAR agonists in cardiovascular diseases. *Am J Cardiovasc Drugs*. 2017;17:273–281. https://doi.org/10.1007/s40256-017-0220-9.

25 Li H, Xue F, Kraus II JM, et al. In search of potent and selective inhibitors of neuronal nitric oxide synthase with more simple structures. *Bioorg Med Chem*. 2013;21:1333–1343. https://doi.org/10.1016/j.bmc.2013.06.014.

26 Liu ZC, Hai YS, Jing W, et al. Discovery and development of novel pyrimidine and pyrazolo/thieno-fused pyrimidine derivatives as potent and orally active inducible nitric oxide synthase dimerization inhibitor with efficacy for arthritis. *Eur J Med Chem*. 2021;213, 113174. https://doi.org/10.1016/j.ejmech.2021.113174.

27 Cinelli MA, Do HT, Miley GP, Silverman RB. Inducible nitric oxide synthase: Regulation, structure, and inhibition. *Med Res Rev*. 2020;40:158–189. https://doi.org/10.1002/med.21599.

28 Entrena A, Camacho ME, Carrión MD, et al. Kynurenamines as Neural Nitric Oxide Synthase Inhibitors. *J Med Chem*. 2005;48:8174–8181. https://doi.org/10.1021/jm050740o.

29 Chayah M, Carrión MD, Gallo MA, Jiménez R, Duarte J, Camacho ME. Development of urea and thiourea kynurenamine derivatives: Synthesis, molecular modeling and biological evaluation as nitric oxide synthase inhibitors. *ChemMedChem*. 2015;10:874–882. https://doi.org/10.1002/cmdc.201500007.

30 Chayah M, Camacho ME, Carrión MD, Gallo MA, Romero M, Duarte J. N, N`-disubstituted thiourea and urea derivatives: Design, synthesis, docking studies and biological evaluation against nitric oxide synthase. *MedChemComm*. 2016;7:667–678. https://doi.org/10.1039/C5MD00477B.

31 Fürstner A, Jumbam DN, Seidel G. Syntheses of Zindoxifene and Analogues by Titanium-Induced Oxo-Amide Coupling. *Chem Ber*. 1994;127:1125–1130. https://doi.org/10.1002/cber.19941270624.

32 Shearer BG, Oplinger JA, Lee S. S-2-Naphthylmethyl Thioacetimidate Hydrobromide: A New Odorless Reagent for the Mild Synthesis of Substituted Acetamidines. *Tetrah Lett*. 1997;38:179–182. https://doi.org/10.1016/S0040-4039(96)02268-X.

33 Ungvari Z, Sun D, Huang A, Kaley G, Koller A. Role of endothelial [Ca2+]i in activation of eNOS in pressurized arterioles by agonists and wall shear stress. *Am J Physiol Heart Circ Physiol*. 2001;281(2):H606–H612. https://doi.org/10.1152/ajpheart.2001.281.2.H606.

34 Fedorov R, Hartmann E, Ghosh DK, Schlichting I. Structural Basis for the Specificity of the Nitric-oxide Synthase Inhibitors W1400 and N$^\omega$-Propyl-l-Arg for the Inducible and Neuronal Isoforms. Structural Basis for the Specificity of the Nitric-oxide Synthase Inhibitors W1400 and N$^\omega$-Propyl-l-Arg for the Inducible and Neuronal Isoforms. *J Biol Chem*. 2003;278:45818–45825. https://doi.org/10.1074/jbc.M306030200.

35 Lipinski CA, Lombardo F, Dominy BW, Feeney PJ. Experimental and computational approaches to estimate solubility and permeability in drug discovery and development settings. *Adv Drug Deliv Rev*. 1997;46(23):3–25. https://doi.org/10.1016/S0169-409X(96)00423-1.

36 Veber DF, Johnson SR, Cheng HY, Smith BR, Ward KW, Kopple KD. Molecular properties that influence the oral bioavailability of drug candidates. *J Med Chem*. 2002;45:2615–2623. https://doi.org/10.1021/jm020017n.

37 Gurung AB, Bhattacharjee A, Ali MA. Exploring the physicochemical profile and the binding patterns of selected novel anticancer Himalayan plant derived active

compounds with macromolecular targets. *Inform Med Unlocked.* 2016;5:1–14. https://doi.org/10.1016/j.imu.2016.09.004.

38 Fukunishi Y, Nakamura H. Definition of Drug-Likeness for compound affinity. *J Chem Inf Model.* 2011;51:1012–1016. https://doi.org/10.1021/ci200035q.

39 Varoli L, Burnelli S, Garuti L, Vitali B. Synthesis and antimicrobial activity of new diazoimidazole derivatives containing an N-acylpyrrolidine ring. *Il Farmaco.* 2011;56 (11):885–890.

40 Bredt DS, Snyder SH. Isolation of nitric oxide synthetase, a calmodulin-requiring enzyme. *Proc Natl Acad Sci U S A.* 1990;87(2):682–685. https://doi.org/10.1073/pnas.87.2.682.

41 Robles-Vera I, Toral M, de la Visitación N, et al. The Probiotic Lactobacillus fermentum Prevents Dysbiosis and Vascular Oxidative Stress in Rats with Hypertension Induced by Chronic Nitric Oxide Blockade. *Mol Nutr Food Res.* 2018;62, e1800298. https://doi.org/10.1002/mnfr.201800298.

42 Morris GM, Huey R, Lindstrom W, et al. AutoDock4 and AutoDockTools4: Automated docking with selective receptor flexibility. *J Comput Chem.* 2009;30:2785–2791. https://doi.org/10.1002/jcc.21256.

43 Hanwell MD, Curtis DE, Lonie DC, Vandermeersch T, Zurek E, Hutchison GR. Avogadro: an advanced semantic chemical editor, visualization, and analysis platform. *J Cheminf.* 2012;4:17. https://doi.org/10.1186/1758-2946-4-17.

44 Frisch MJ, Trucks GW, Schlegel HB, Scuseria GE, Robb MA, Cheeseman JR, Scalmani G, Barone V, Mennucci B, Petersson GA, Nakatsuji H, Caricato M, Li X, Hratchian HP, Izmaylov AF, Bloino J, Zheng G, Sonnenberg JL, Hada M, Ehara M, Toyota K, Fukuda R, Hasegawa J, Ishida M, Nakajima T, Honda Y, Kitao O, Nakai H, Vreven T, Montgomery Jr JA., Peralta JE, Ogliaro F, Bearpark M, Heyd JJ, Brothers E, Kudin N, Staroverov VN, Keit T, Kobayashi R, Normand J, Raghavachari K, Rendell A, Burant JC, Iyengar SS, Tomasi J, Cossi M, Rega N, Millam JM, Klene M, Knox JE, Cross JB, Bakken V, Adamo C, Jaramillo J, Gomperts R, Stratmann RE, Yazyev O, Austin AJ, Cammi R, Pomelli C, Ochterski JW, Martin L, Morokuma K, Zakrzewski VG, Voth GA, Salvador P, Dannenberg JJ, Dapprich S, Daniels AD, Farkas O, Foresman JB, Ortiz JV, Cioslowski J, Fox DJ. GAUSSIAN 09 (Revision D.1), GAUSSIAN 09 (Revision B.01); 2010.

45 Dolinsky TJ, Nielsen JE, McCammon JA, Baker NA. PDB2PQR: an automated pipeline for the setup of Poisson-Boltzmann electrostatics calculations. *Nucleic Acids Res.* 2004;32:W665–W667. https://doi.org/10.1093/nar/gkh381.